Journal of Nuclear Materials 380 (2008) 70–75

Contents lists available at ScienceDirect

Journal of Nuclear Materials

journal homepage: www.elsevier.com/locate/jnucmat

Strain evolution of zirconium hydride embedded in a Zircaloy-2 matrix

M. Kerr [a], M.R. Daymond [a,*], R.A. Holt [a], J.D. Almer [b]

[a] Department of Mechanical and Materials Engineering, Queen's University, Kingston, ON, Canada K7L 3N6
[b] Advanced Photon Source, Argonne National Laboratory, Argonne, IL 60439, USA

ARTICLE INFO

Article history:
Received 13 May 2008
Accepted 14 July 2008

ABSTRACT

In situ synchrotron X-ray diffraction has been used to determine strain evolution in a minority phase, zirconium hydride, embedded in Zircaloy-2 (<100 wt ppm average hydrogen content). The elastic modulus of the hydride is similar to that of Zircaloy-2. Three regimes are observed: I – elastic, II – post-yield load transfer from Zircaloy-2 to hydride, and III – strain saturation, possibly due to hydride fracture. The interpretation is supported by finite element calculations and scanning electron microscopy of the fracture surface.

1. Introduction

Zirconium and its alloys are used in the nuclear industry world wide because their combination of low neutron capture cross section, good mechanical properties, and corrosion resistance make them uniquely suited for in-reactor applications. Hydrogen uptake in zirconium components during service is problematic as the solubility of hydrogen in zirconium is low and brittle hydride phases can form, degrading the mechanical properties. In Canada Deuterium Uranium (CANDU[©1]) pressurized heavy water reactors, degradation of the Zr2.5Nb pressure tubes by a thermally assisted slow cracking mechanism (delayed hydride cracking – DHC) occurs at hydrogen concentration less than 100 parts per million by weight (wt ppm) [1]. In reactors world wide hydrides are a concern for Zircaloy fuel sheathing, particularly in high burn-up conditions, when hydrogen concentrations in the range of 100–1000 wt ppm can produce brittle failure of the fuel sheathing under mechanical load [2]. Hydride formation also occurs in several other metal hydrogen systems (titanium, niobium, and vanadium) [3,4], and the embrittlement observed in the titanium hydrogen system is similar to that observed in zirconium [4].

The investigation of zirconium hydrides presents several challenges, most specifically isolating a hydride (or hydrides) for mechanical testing. Typical methods for investigating properties of the hydrides are preparation of a macroscopic 'bulk' hydride sample [5,6], mechanical tests of hydrided material with hydride response inferred from acoustic emission [7–11], and growth of a large hydride in a zirconium matrix for indentation experiments [6]. These techniques do not provide a complete description of the mechanical response of hydrides embedded in a zirconium matrix. Rather, different techniques have their strength in studying a particular facet of hydride mechanical behavior. Tests on bulk hydrides can provide information on both elastic and plastic properties, but it is difficult to grow a defect free crystal, potentially introducing experimental artifacts to the data set. Further, the microstructure of bulk crystals is quite different from hydrides precipitated in a zirconium matrix [6]. Acoustic emission can be used directly on hydrided material, finding application in identifying when hydrides fracture during a mechanical test, but providing no direct data on the elastic and plastic properties of the hydride or on the local stress state causing fracture.

One of the major findings from acoustic emission studies has been that hydride fracture can occur near the onset of tensile loading, typically peaking after some amount of plastic deformation in the zirconium matrix [9,10]. When loading is bi-axial or tri-axial, the critical strain required for hydride fracture is reduced [7–11] compared with uni-axial loading. Experiments on bulk hydride crystals indicate that the hydride elastic modulus is similar to that of zirconium, but the fracture behavior of these crystals is difficult to interpret because the behavior of the brittle hydride is governed by its defect population [5,6]. Indentation experiments on large hydrides grown in zirconium also suggest that the elastic modulus of the hydride phase is similar to that of zirconium. These measurements tend to be scattered, with the scatter attributed to the possibility of indenting different crystallographic orientations of the hydride [6].

Here we use the technique of synchrotron X-ray diffraction to measure the response of the minority hydride phase in situ, and interpret the response using composite mechanics.

2. Experimental procedures

Samples were produced from a section of warm-rolled Zircaloy-2 slab with a 20 μm grain size. The texture and mechanical properties of the plate have been well characterized [12]. A slice measuring

* Corresponding author.
E-mail address: daymond@me.queensu.ca (M.R. Daymond).

[1] CANDU is the registered trademark of Atomic Energy of Canada Ltd.

0022-3115/$ - see front matter © 2008 Elsevier B.V. All rights reserved.
doi:10.1016/j.jnucmat.2008.07.004

$2.25 \times 30 \times 60\ mm^3$ was machined from the plate and electrolytically hydrided at room temperature in a solution of sulfuric acid for 24 h (producing maximum hydride layer thickness without spalling) [13]. Following the deposition of the hydride layer, samples were homogenized at 500 °C for 12 h, yielding a hydrogen concentration in solution of ~90 wt ppm, as measured by differential scanning calorimetry on a small button punched from the specimen. The slice was then cooled to ambient at 1 °C/min producing a typical furnace cooled hydride microstructure [1], with $2 \times 20 \times 20\ \mu m^3$ hydride 'cornflakes' tending to precipitate in the rolling/transverse plane of the plate. This hydride orientation is attributed to the strong basal texture along the normal direction of the plate produced on rolling (Fig. 1) [14].

The thickness dimension of 2.25 mm was selected as a compromise between (a) good X-ray penetration, (b) providing diffraction signal from a significant number of hydrides and (c) readily obtaining sufficient hydrogen concentration – the thinner the plate the greater the hydrogen concentration that can be easily achieved. The hydrided slice was cut into compression and tension samples. For compression, samples of dimension $4 \times 3 \times 2.25\ mm^3$ were cut with the loading axis in all three principle directions (transverse (TD), rolling (RD), normal (ND)). For tension, only TD and ND orientations could be cut parallel to the loading direction, with a gage of $7 \times 1 \times 2.5\ mm^3$.

High-energy X-ray diffraction measurements were conducted at the 1-ID beamline at the Advanced Photon Source (Argonne National Laboratory, IL) [15]. Tensile and compressive loads were applied to the specimens using a custom built stepper motor driven load frame [16,17]. The stepper motor position was incrementally increased during the course of a test and then held. After a 30 s dwell at each position to allow for load relaxation a diffraction measurement was made [14]. Diffraction measurements were performed with monochromatic 81 keV ($\lambda = 0.015$ nm) X-rays in transmission with a beam size of $200 \times 200\ \mu m^2$.

As the hydride phase is a minority phase in the Zircaloy-2 matrix, the diffraction signal from the hydride was maximized by (1) detector selection, (2) total exposure time, (3) sample translation, and (4) detector position. The $40 \times 40\ cm^2$ GE amorphous silicon detector used in this study allowed rapid capture and reading of the Debye–Scherrer diffraction rings. To increase the signal from the minority hydride phase, ten 1.25 s exposures were taken and summed together, with the maximum single exposure time set to just avoid detector saturation of the strongest zirconium peak. Collecting more exposures than ten did not decrease the uncertainty in fitting to the hydride phase, indicating that a stable peak to background ratio was reached. Also, a single exposure required ~8 MB memory, making data management a concern. In order to obtain a suitable sampling of the hydride population during the course of the test, a sequence of exposures was made while translating the sample over roughly 1 mm. This effectively increased the sampling volume by a factor of five, minimizing the potential for sampling artifacts as a population of hydrides moved in or out of the beam during loading. Finally, the detector-to-sample distance was set at 1995 mm, compromising between the number of peaks that could be measured and the strain resolution in the hydride phase. This yielded coverage of five zirconium peaks from $\{1\bar{1}20\}$ to $\{10\bar{1}0\}$.

Diffraction patterns were extracted from circumferentially summed Debye–Scherrer rings [16–18], i.e., diffraction patterns were obtained at nominal angles around the ring of 0°, 90°, 180°, and 270°, integrating ±10° around the nominal direction. The equivalent scattering vectors within the sample were then averaged (i.e. 0°/180° and 90°/270°), producing diffraction patterns corresponding to scattering vectors parallel to and perpendicular to the loading direction. An example diffraction pattern is shown in Fig. 2. Note that there are five strong zirconium peaks, while the inset shows the only individually resolvable hydride peak, {1 1 1}, neighboring the $\{10\bar{1}0\}$ zirconium peak. Other hydride peaks overlap strongly with zirconium peaks, and could not be individually resolved to allow unambiguous peak fitting. The low intensity of the hydride phase is principally a result of the low concentration of hydrogen in the material (~90 wt ppm). Fitting of the {1 1 1} hydride peak/$\{10\bar{1}0\}$ zirconium peak pair, as well as the other zirconium peaks, was accomplished using the single peak fitting routine within the GSAS software package [19]. A pseudo-Voigt peak shape was used with the Gaussian width allowed to vary but the Lorentzian component of the width defined from a calibration sample. Changes in the lattice parameter obtained from the fit were used to determine strain components ε_{xx} and ε_{yy}.

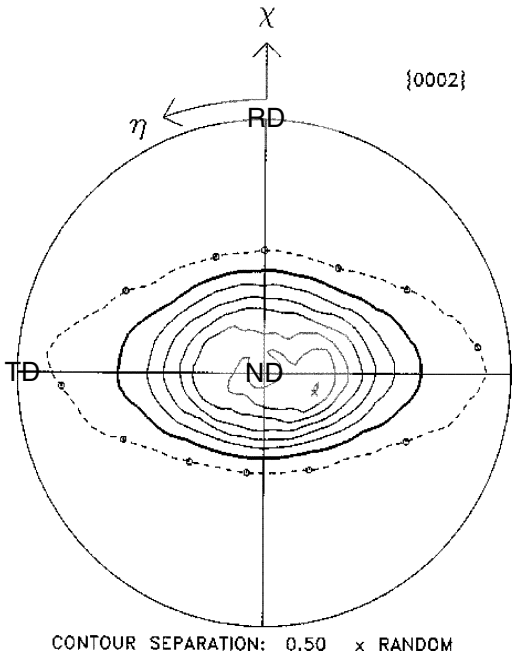

Fig. 1. {0002} Pole figure for the Zircaloy-2 plate showing the strong alignment of basal poles along the normal direction (ND) to plate rolling, this texture influences hydride precipitation (Max MRD ~3.75).

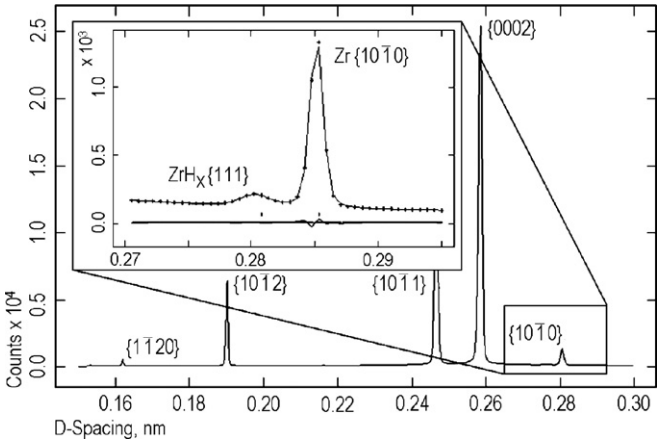

Fig. 2. Diffraction pattern produced after binning Debye–Scherrer rings over 20°. Inset shows the resolvable hydride {1 1 1} and neighboring diffraction peak, as well as the fit to the diffraction data.

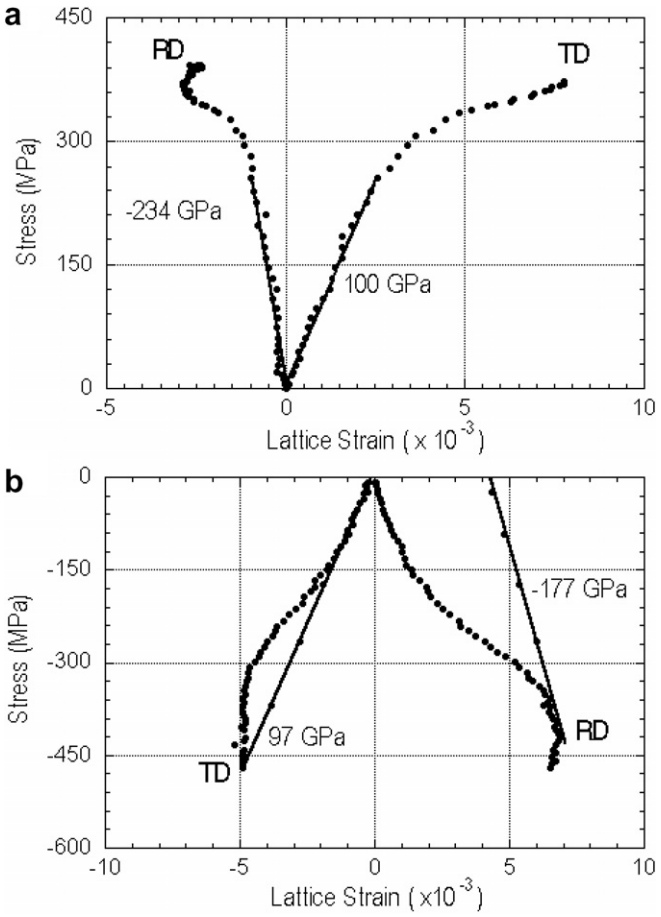

Fig. 3. Applied stress versus lattice strain evolution for the {1 1 1} hydride peak for samples loaded axially along TD in (a) tension and (b) compression. RD is perpendicular to applied load in both cases. The strain components both parallel (TD) to loading and perpendicular to loading (RD) are plotted.

3. Results

The data obtained for the samples with load applied parallel to the transverse direction (TD) of the plate is plotted in Fig. 3. The lattice strain evolution for the {1 1 1} hydride peak is shown as a function of applied stress, as measured by load cell during the experiment. The lattice strain evolution observed was qualitatively similar for all sample orientations, and will thus be examined in detail. We note that the lattice strain for the hydride phase shows three distinct regimes: (Regime I) an initial linear region, (Regime II) a second linear region initiated by an inflection, with a subsequent decrease in slope, and (Regime III) a second inflection followed by strain saturation. This qualitative division of behavior is observed in both tension and compression for all sample orientations. There is a statistical uncertainty of ±70 μstrain on each data point which propagates to an uncertainty of ±10% in the elastic modulus values reported. Elastic moduli values (Regime I) and the stresses associated with transitions between regimes (Regimes I/II and Regimes II/III) for the different experimental runs are summarized in Table 1.

There are two experimental features of the data that should be noted. First, the anisotropy in the stress value of the Regime I/II transition seen in tension and compression for a given sample orientation is too large to be explained by the usual anisotropy in yield stress observed in Zircaloy-2 [12]. This may be due to the difficulty of ensuring parallel surfaces of the compression samples and therefore the values for this transition in compression should be treated with caution. The Regime II/III transition occurs at approximately the same stress in both tension and compression and should be largely free of sample geometry artifacts as it occurs after significant plastic deformation. Further the elastic modulus values measured on unloading after compression should also be free of this artifact and are reported in Table 1. Second, during tensile loading peak overlap occurs in the axial data set between the hydride (Zr_xH {1 1 1}) and zirconium (Zr {1 0 $\bar{1}$ 0}) diffraction peaks, starting at a stress somewhat above the Regime I/II transition. This overlap was observed for both of the samples measured in tension and means that the hydride diffraction peak cannot be observed reliably for high applied stresses. Thus we cannot identify a Regime II/III transition in the direction parallel to the applied load; however the signature of the Regime II/III transition is observed in the data sets perpendicular to the loading direction (Fig. 3). Therefore these perpendicular banks are used to estimate the stress and strains of the Regime II/III transition in Table 1 for tensile samples. This effect is only seen in tension due to the sense of the strains generated in the hydride (Zr_xH {1 1 1}) and zirconium (Zr {1 0 $\bar{1}$ 0}) diffraction peaks relative to their initial d-spacing.

4. Discussion

4.1. Lattice strain evolution

The three regions observed in the hydride strain evolution appear consistent with (Regime I) elastic loading, (Regime II) load transfer to the hydride phase after yield of the Zircaloy-2 matrix, and (Regime III) strain saturation in the hydride. In the initial elastic region, a hydride elastic modulus of ~100 GPa is determined

Table 1
Summary of results from the Zr_xH {1 1 1} hydride peak for all tension and compression runs

Orientation parallel/perpendicular to axial loading	Regime I (elastic moduli)	Transition between Regimes I/II (start of load transfer)	Transition between Regimes II/III (start of strain saturation)	Strain saturation values	
				Parallel to applied load ε_{xx} (10^{-6})	Perpendicular to applied load ε_{yy} (10^{-6})
	GPa	MPa	MPa		
Tension					
TD/RD	100.9 ± 10.1	267.3 ± 7.1	349.1 ± 7.1	*6294 ± 70*	−2585 ± 83
ND/RD	115.1 ± 11.5	439.5 ± 8.0	469.9 ± 8.0	*5218 ± 70*	−1532 ± 83
Compression					
TD/RD	97.0 ± 9.7	−150 ± 6.8	−324 ± 6.8	−4679 ± 70	5650 ± 83
RD/TD	78.0 ± 7.8	−142.2 ± 5.4	−222.5 ± 5.4	−4349 ± 70	4549 ± 83
ND/RD	95.9 ± 9.6	−313.1 ± 6.7	−444.0 ± 6.7	−5757 ± 70	4834 ± 83

Included are the hydride elastic moduli (Regime I), transition stresses between the three regimes observed, and microstrain values at saturation in the direction parallel (x) and perpendicular (y) to the applied load.
Note: Numbers in italics indicate estimates from transverse banks, as peak overlap occured in the axial banks under tension (see Section 3).

(97 ± 13 GPa based on the average of the values given in Table 1). This is consistent with experiments conducted on bulk hydrides and indentation experiments [6], and similar to the elastic modulus of zirconium.

4.2. Load transfer to hydride phase

A 2-dimensional plane stress finite element model was constructed, which confirmed that the inflection in hydride lattice strain at the transition between Regimes I/II could be explained by load transfer from the zirconium matrix. Dimensions for the hydride precipitate were estimated from optical metallography, which revealed that the hydrides were approximately 20 μm in length, with an aspect ratio of 10:1, and had ~5% area fraction TD/ND and RD/ND planes. Unit cell boundary conditions were set to model a regular infinite array of such hydrides. It should be noted that the area fraction estimated from metallography is higher than the ~1% estimated from hydrogen charging, probably due to the etching process. This is not expected to significantly influence results of the model, as there do not appear to be hydride/hydride stress field interactions. In the absence of these interactions, the hydride aspect ratio should be the dominant effect in load transfer to the hydride phase (see Section 4.3). Both the hydride and the Zircaloy-2 matrix were given an elastic modulus of 100 GPa, while only the Zircaloy-2 matrix was assumed to plastically deform. Tensile tests conducted on un-hydrided Zircaloy-2 samples from the same plate used in this study were used as input stress–strain curves for the model and to calculate Hill parameters to account for the plastic anisotropy of the Zircaloy-2 matrix. Results of the calculation for axial loading along TD are shown in Fig. 4, with good agreement between the model and data set. The elastic strain from the FE calculation is compared to the lattice strain for the Zircaloy-2 matrix using the average of the five Zircaloy-2 peaks [20] and the lattice strain for the {1 1 1} hydride peak. An average strain from five Zircaloy-2 peaks was used to minimize the effect of elastic and plastic anisotropy [20]. Such averaging was not carried out for the hydride since only one peak was accurately measured, however the strain should be representative of the average elastic response if the elastic anisotropy of the phase is assumed to be small and no plastic anisotropy is expected. Both phases show an elastic response until yielding of the matrix occurs. At this point, the elastic strain in the Zircaloy-2 matrix stops increasing with increasing applied stress and load is transferred to the plastically harder hydride phase.

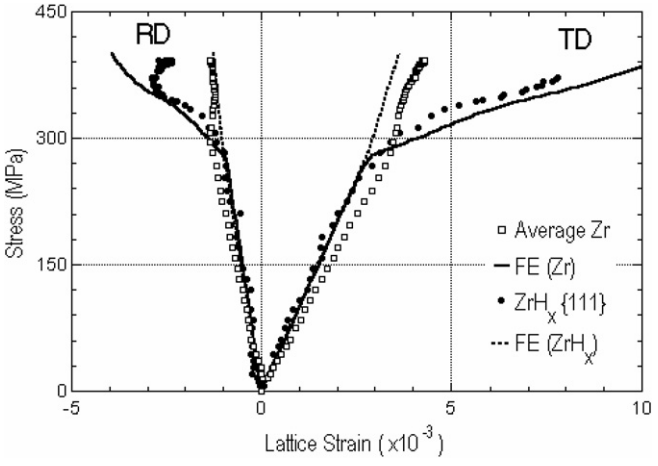

Fig. 4. Results from the FE calculation compared to the experimental data for both phases, under applied tension. Sample is loaded along TD, with RD perpendicular to the applied load.

These details agree well between model and experiment, confirming the occurrence of load transfer prior to fracture in this material.

4.3. Hydride fracture

There are a number of possible explanations for Regime III, i.e., the strain saturation that occurs after the region of load transfer. Potential sources for saturation of strain in the hydride phase include (1) hydride fracture, (2) interface failure, (3) plastic deformation of hydrides, or (4) work hardening around the hydride leading to load transfer back to the matrix. Interface failure is highly unlikely as to date there is no evidence for its occurrence and only hydride fracture has been observed [10]. Work hardening close to the Zircaloy-2/hydride interface should occur as a result of localized plasticity, but the work hardening rate in this annealed Zircaloy-2 plate is relatively low [12] and is unlikely to be high enough to account for strain saturation. The onset of the saturation is rapid and we would expect a more gradual transition and less steep final gradient if matrix hardening was responsible. We note in passing that this effect could be studied further experimentally by using zirconium alloys with different work hardening characteristics as the parent material for the hydride phase.

Orientation relationships for slip for hydrides in zirconium have not been reported, but bulk zirconium hydride appears to slip on {1 1 1} [5]. Plastic deformation has been reported to occur in hydrides in a zirconium matrix at both room and elevated temperature, but only in a minority of the hydrides present. For slip to occur hydrides must precipitate within a grain and be favorably oriented relative to the surrounding zirconium grains and this orientation is not the case for the vast majority of hydrides in zirconium [11,21]. Further, hydride precipitation at grain boundaries is common and slip has not been observed in these hydrides [11]. Diffraction strain measurements are the average response of the grains oriented for diffraction, therefore if the observed saturation is a result of hydride plasticity the majority of the hydrides in the material would have to plastically deform. This interpretation is not consistent with the literature [2,5–11,21] hence we expect the average response of the hydrides in zirconium to be brittle to failure.

Acoustic emission experiments conducted on hydrided zirconium indicate that hydride fracture occurs throughout the course of a tensile test, typically peaking between 1% and 4% matrix plastic strain depending on alloy composition and stress state [7–10]. Hence we suggest that the observed Regime III strain saturation represents a stable regime where the stress in the hydrides cannot be further increased. This limit would be due to a combination of limited plastic hardening in the zirconium matrix, but more importantly, the fracture of the hydride particles to an average size below which they can no longer fracture. The transition from Regime II to Regime III behavior occurs at approximately 3% matrix plastic strain in the current study. This type of behavior has been reported in conventional composite materials and can be understood through a shear lag model [22,23]. In a shear lag model description, for hydrides below some critical length (the stress transfer length (l_t)), a peak stress is reached in the center of the hydride wherein the peak stress is a function of hydride length. Above the stress transfer length, the stress instead plateaus in the center of the fiber at a value which is independent of the size of the hydrides and depends only on elastic properties of the phases. Hence if the hydride is significantly longer than l_t, the *average* stress in the hydride is relatively insensitive to the length of the fiber. In a diffraction experiment the initial hydride fractures detected with acoustic emission would not be observed, provided that after fracture the hydrides' length still significantly exceeded the stress transfer length. This is because if this condition is met, the average load transferred to the hydride phase is essentially unchanged by

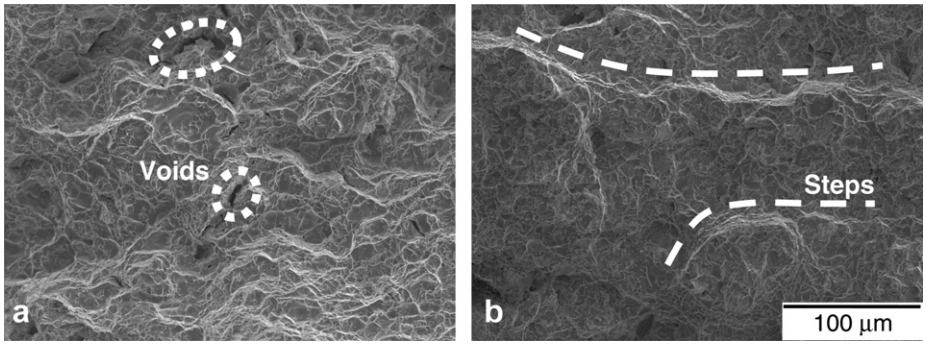

Fig. 5. SEM micrographs of the tensile fracture surfaces (a) TD and (b) ND.

fracture, and hence the average hydride strain response as measured by diffraction is also unchanged. As the hydrides continue to fracture, the average hydride length will eventually decrease below the critical stress transfer length. At this point, the average stress born by the hydride phase will decrease with further fracture. Therefore, the strain saturation observed at the Regime II/III transition likely represents a critical hydride length, the failure length (l_f), where the hydrides can no longer be loaded due to fracture.

It is possible to roughly estimate the stress transfer length and the failure length for hydrides oriented with their plate normal perpendicular to the loading direction (loading along TD or RD). The stress transfer length is estimated as [22]

$$l_t = \frac{3t}{n},$$

where t is the hydride thickness (~2 μm) and n is a dimensionless constant related to the stress distribution in the hydride. As the elastic constants of the hydride and matrix appear equal n is approximated as unity, yielding a stress transfer length of ~6 μm. This length is significantly less than the initial length of the hydrides (~20 μm), consistent with the proposed fracture mechanism.

Assuming the transition to Regime III strain saturation occurs because the hydrides have fractured to the failure length, at low volume fractions the failure length for hydrides along the orientation described above is estimated as [23]

$$l_f = \frac{\sigma_H}{\tau_H}\left(\frac{t}{2}\right),$$

where σ_H is the axial stress required to fracture the hydride, τ_H is the interfacial friction stress, and t is the thickness of the hydride. Estimating σ_H from our finite element model results (~800 MPa) and approximating the Zircaloy-2 interface strength with a Tresca criterion ($\tau_H \sim \frac{1}{2}\sigma_y$), yields a failure length of ~4.5 μm. Our analysis assumes that the Regime III strain saturation occurs because the hydrides have fractured to lengths at or below the stress transfer length (with fracture starting during Regime II) and therefore can no longer be loaded to a higher load. The estimate then represents the expected hydride size post specimen tensile rupture and correlates well with microscopic studies of fractured hydrides reported in the literature [9]. This explanation does require a reasonably wide population of defects to be present in the hydrides; the distribution of strength-limiting defects in zirconium hydride is unknown. It must be noted that the above treatment is not sufficient to directly explain the behavior of hydrides with plate normal oriented parallel to the loading direction (loading along ND), as the hydrides are ~2 μm thick and not sufficiently long to sustain a shear lag loading mechanism. Given that a shear lag loading cannot operate, load transfer to these hydrides must be less efficient and, qualitatively would be expected to provide a contribution to the higher transitions Regime I/II and Regime II/III observed for samples loaded along ND relative to those loaded along RD and TD (Table 1). More complex finite element or Eshelby type models would be required to capture the details of the load transfer behavior for hydrides with plate normal parallel to loading.

To confirm the occurrence of hydride fracture, the fracture surface of the tension specimens (TD and ND axial orientations) were examined by SEM. In the TD orientation hydride precipitates are acicular in cross section (~2 × 20 μm^2), while in the ND orientation they appear as plates. Fig. 5(a) is a micrograph of the TD orientation and reveals voids in the fracture surface with the approximate dimensions of the expected hydrides. The ND orientation in Fig. 5(b) reveals steps in the fracture surface, likely as a result of the fracture of hydride plates. Linking of hydride plate initiation sites produces a 'stepped' fracture surface. With the exception of the voids present in the TD orientation and the steps present in the ND orientation, the fracture surfaces have the ductile character expected for Zircaloy-2. These features (voids and steps) are the characteristic features of hydride fracture [2,7,8].

The analysis carried out in this work has established the possibility of minority phase stress analysis. While data quality and signal from the hydride phase could be improved by increasing the hydrogen concentration, the low concentrations studied in this experiment (<100 wt ppm) are of technical importance for DHC [1]. A future study to greater hydrogen concentrations (100–1000 wt ppm) would be of interest to study the effects of increased hydride volume fraction, as well as the potential of fitting other hydride peaks in order to investigate potential elastic anisotropy of the phase. These higher concentrations are of technical importance for fuel sheathing embrittlement [2].

5. Conclusions

The following conclusions are drawn regarding the strain evolution in hydrides embedded in a Zircaloy-2 matrix:

- Strain measurements can be made in zirconium hydrides at low hydrogen concentrations (<100 wt ppm) using synchrotron X-ray diffraction.
- The moduli of the hydride and Zircaloy-2 matrix are similar, having a magnitude of ~100 GPa.
- FE calculations show that load transfer to the harder hydride phase is responsible for the first inflection post Zircaloy-2 yield (Region I/II transition) observed in the diffraction data for the hydride phase.
- The strain saturation observed in the hydride could be a result of hydride fracture. This is supported by microscopy and consistent with composite load transfer models.

Acknowledgements

Work supported by NSERC, COG, OPG and Nu-Tech Precision Metals under the Industrial Research Chair Program in Nuclear Materials at Queen's University. Use of the Advanced Photon Source was supported by the US Department of Energy, Office of Science, Office of Basic Energy Sciences, under Contract DE-Ac02-06CH11357. The authors would like to thank AECL Chalk River Labs for assistance with sample hydriding and metallography. M. Kerr would like to thank his colleague Feng Xu for useful discussions (data set comparisons and modeling).

References

[1] D.O. Northwood, U. Kosasih, Int. Met. Rev. 28 (1983) 92.
[2] J.B. Bai, C. Prioul, D. Francois, Metall. Mater. Trans. A 25 (1994) 1185.
[3] M.P. Puls, Acta Metall. 32 (1984) 1259.
[4] N.E. Paton, J.C. Williams, Effect of Hydrogen on Titanium and its Alloys, in: I.M. Bernstein, A.W. Thompson (Eds.), Hydrogen in Metals, vol. 2, American Society for Metals, Metals Park, OH, 1974, p. 409.
[5] K.G. Barraclough, C.J. Beevers, J. Mater. Sci. 4 (1968) 518.
[6] M.P. Puls, S.Q. Shi, J. Rabier, J. Nucl. Mater. 336 (2005) 73.
[7] L.A. Simpson, Metall. Trans. A 12 (1981) 2113.
[8] M.P. Puls, Metall. Trans. A 19 (1988) 1507.
[9] M.P. Puls, Metall. Trans. A 22 (1991) 2327.
[10] R. Choubey, M.P. Puls, Metall. Mater. Trans. A 23 (1994) 993.
[11] M. Grange, J. Besson, E. Andrieu, Metall. Mater. Trans. A 31 (2000) 679.
[12] F. Xu, R.A. Holt, M.R. Daymond, J. Nucl. Mater. 373 (2008) 217.
[13] A.D. Lepage, W.A. Ferris, G.A. Ledoux, Procedure for Adding Hydrogen to Small Sections of Zirconium Alloys, IAEA Report FC-IAEA-03, published as Appendix 3 of IAEA-TECDOC-1410, 2004.
[14] F. Xu, R.A. Holt, M.R. Daymond, R.B. Rogge, E.C. Oliver, Mater. Sci. Eng. A 488 (2008) 172.
[15] D.R. Haeffner, J.D. Almer, U. Lienert, Mater. Sci. Eng. A 399 (2005) 120.
[16] A. Warner, D.C. Dunand, Metall. Mater. Trans. A 31 (2000) 2949.
[17] M.R. Daymond, M.L. Young, J.D. Almer, D.C. Dunand, Acta Mater. 55 (2007) 3929.
[18] M.R. Daymond, P.J. Withers, Scr. Mater. 35 (1996) 1229.
[19] A.C. Larson, R.B. Von Dreele, General Structure Analysis System (GSAS), Los Alamos National Laboratory Report LAUR 86-748, 2000.
[20] M.R. Daymond, J. Appl. Phys. 96 (2004) 4263.
[21] C.E. Coleman, D. Hardie, J. Less Common Met. 11 (1966) 168.
[22] D. Hull, T.W. Clyne, An Introduction to Composite Materials, Cambridge Solid State Science Series, Cambridge University Press, UK, 1996.
[23] A. Kelly, N.H. Macmillan, Strong Solids, Oxford University Press, UK, 1987.